Preparation and Characterization of Nitrogen and Oxygen Heteroatom Codoped Activated Biocarbons from Edamame Shell

Tingting Chen,[a] Lu Luo,[a] Zeliang Li,[a] Zhicheng Zhang,[a] Shouwen Zheng,[a] Zhicheng Zhu,[a] Ju He,[b,*] and Weigang Zhao [a,*]

A simple procedure was evaluated to prepare cost-effective heteroatom self-doped porous carbons from edamame shell using a two-step carbonization and activation process. The morphological, structural, textural properties and N_2/CO_2 adsorption–desorption were investigated. The results showed that edamame shell, which is abundant in nitrogen and oxygen, is an ideal precursor for preparing heteroatom self-doped porous carbons. The N and O contents of the prepared activated carbons (ACs) ranged from 1.20 wt% to 1.81 wt% and 5.13 wt% to 9.98 wt%, respectively. Furthermore, the specific surface area of 1835 m^2/g of the N and O doped ACs resulted in mainly microporosity, which suggested that it has promising potential for wide applications in the fields of catalysis, energy conversion, energy storage devices, and adsorption.

INTRODUCTION

Carbon-based materials have attracted considerable interest for many energy- and environment-related applications, such as supercapacitors (Hwang *et al.* 2017), batteries (Tai *et al.* 2017), hydrogen storage (Luo *et al.* 2017), fuel cells (Zhang *et al.* 2011), CO_2 capture (Zhao *et al.* 2017a), and water pollution treatment (Liu *et al.* 2014). This high level of interest can be attributed to their abundance, chemical and thermal stability, processability, and textural and structural tunability to fulfill the requirements of specific applications. In particular, activated carbon (AC) is an allotrope of disordered carbon materials that is distinguished for its high specific surface area and microstructure porous system, and stability for large-scale production (Karnan *et al.* 2016; Zhao *et al.* 2017b).

Activated carbons can be produced from any inexpensive material that has a high C content and moderate inorganic content, such as degraded or fossil biomass (*e.g.*, peat, lignite, and all ranks of coal) and fresh biomass (*e.g.*, wood, coconut shells, *etc.*). They can be produced using physical activation with different oxidizing gases, such as air, O_2, CO_2, steam, and their mixtures, or through chemical activation with KOH, NaOH, H_3PO_4, $ZnCl_2$, and other chemical compounds (Şahin and Saka 2013; Ahmad *et al.* 2014). It is also well known that, although the surface of ACs is primarily non-polar, some surface functional groups do exist that play a very important role and influence their performance in the final application (Yamashita *et al.* 2006; Dang *et al.* 2017; Jiang *et al.* 2017).

Among ACs, N- and/or O-doped ACs have gained increasing interest over the last decade, mainly because doping carbonaceous materials with the heteroatoms is an effective way to modify their surface chemistry and improve their application performance (Hulicova-Jurcakova *et al.* 2009; Meng *et al.* 2014; Alabadi *et al.* 2016; Li *et al.* 2017; Ma *et al.* 2017; Ye *et al.* 2017). The N and O are predominantly introduced by one of two ways to fabricate N/O-doped ACs, which are carbonization/activation of N/O-enriched precursors and post-treatment with a N/O source, such as urea, melamine, ozone, plasma oxidation, *etc.* (Boudou 2003; Hulicova-Jurcakova *et al.* 2009; Xia *et al.* 2011; Zhao *et al.* 2013; Zhai *et al.* 2016). However, a negative impact of the post-treatment has been demonstrated by several authors because of the decreasing of the specific surface area by the pore blocking. Therefore, reasonable efforts have been devoted to developing heteroatom self-doped carbon materials from biowaste because of the low cost and simple procedure (Gao *et al.* 2015; Xu *et al.* 2015; Gao *et al.* 2016).

The symbiotic nitrogen fixation of legumes with *Azotobacter* has been a hot topic of scientific research that attracted the attention of the authors because of the much higher N content in their stems and shells compared with other biomass materials (Wani *et al.* 1995; Ci and Gao 2005). Legumes and especially edamame, which originates from China, have a high global annual production (Ren *et al.* 2011). Most edamame shells are a large-quantity by-product; however it is usually abandoned or sintered, which is harmful to the environment. The most important, but often ignored, characteristic of edamame shell is that it is rich in carbon, oxygen, and nitrogen.

This present work used edamame shell as a raw material to prepare heteroatom self-doped activated carbons and KOH as the activation agent. This material would not only generate value-added products from agriculture waste but also offer a potentially cost-effective alternative to ACs precursors. The aim of this experiment was to investigate the impact of the weight ratio of KOH/ edamame shell charcoal and to characterize the N and O dual doped ACs from edamame shell.

EXPERIMENTAL

Materials

Edamame shell (vegetable soybean shell) was used as a carbon precursor, and it was obtained from a commercial plantation area in Fuzhou, Fujian, China. It was repeatedly cleaned with tap water to remove impurities, placed in the sun for three days to remove most of the water, and then placed in an oven at 105 °C for 24 h to remove the residual moisture. All of the reagents, including KOH and HCl, were of analytical grade and used without further purification or treatment.

Activated carbon synthesis

The edamame shell was put into ceramic pots and then placed in a muffle furnace under a pure N_2 environment. The furnace was heated from room temperature to 450 °C at a heating rate of 5 °C/min. The target temperature was maintained for 1 h. The N_2 flow rate was 300 mL/min. The furnace was cooled down to room temperature under a N_2 atmosphere, and the edamame shell charcoal (BS) was finally obtained.

The BS was ground and sieved to generate a uniform powder with particle sizes that ranged from 120 μm to 200 μm. The BS powder and KOH pellets were then mixed at KOH/BS weight ratios (*W*) of 2, 3, 4, 5, and 6. They were placed in a muffle furnace under

a pure N_2 atmosphere, the temperature was increased from room temperature to 800 °C, and the target temperature was maintained for 2 h. The whole process was conducted under a stream of N_2 with a flow rate of 300 mL/min. The crucible was then allowed to cool down to room temperature. The activated product was first washed with 1 M HCl, then with distilled water, and finally with a Soxhlet extractor with a low-temperature cooling circulating pump for three days. Pure activated carbons (BC) were obtained after drying in an oven for 24 h. The schematic procedure of the complete synthesis route of N/O-doped porous carbon from edamame shell is shown in Fig. 1.

All of the prepared BCs were as labeled BCxx. In this nomenclature, the xx at the end refers to the *W*. For example, BC13 means that the BS/KOH *W* was 1:3.
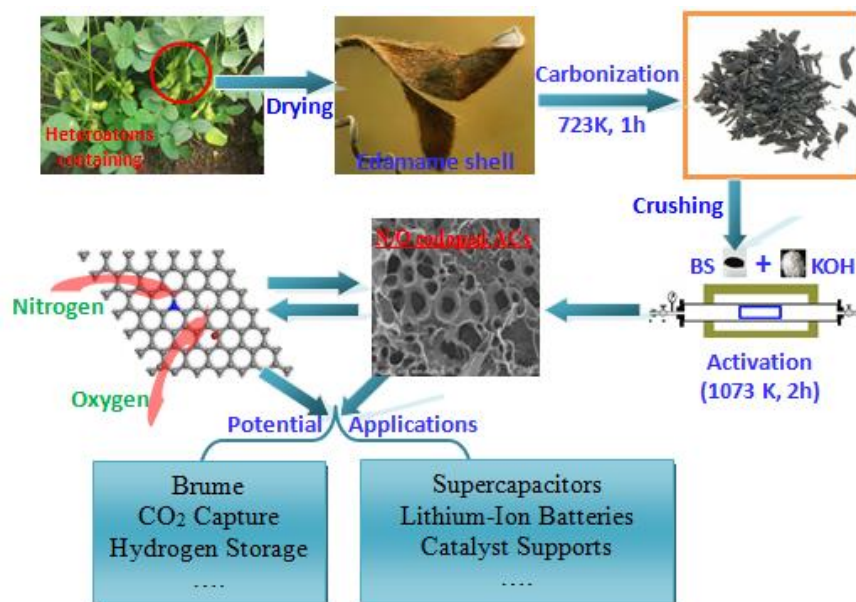

Fig. 1. Schematic procedure of the complete synthesis route of the N/O-doped porous carbons from edamame shell

Analysis Method

Physicochemical characterization of the materials

The TG curves representing the carbonization and activation processes at a *W* value of 3 were obtained by means of thermogravimetric analysis (TGA; SDT-Q600, NETZSCH-Gerätebau GmbH, Wittelsbacherstraße, Germany). The samples were heated from room temperature to a final temperature of 1273 K at a rate of 10 K/min under a N_2 atmosphere with a flow rate of 20 mL/min.

The surface morphology of the samples was determined using scanning electron microscopy (SEM; FEG SEM Hitachi S 3400, Chiyoda-ku, Tokyo, Japan) and high-resolution transmission electronic microscopy (HRTEM; JEM-2100, JEOL, Tokyo, Japan) at an accelerating voltage of 200 kV.

The elemental analysis was performed with a Vario EL elemental analyzer (Elementar, Langenselbold, Germany) and X-ray photoelectron spectrometer (XPS; SPECS XPS System, Surface Nano Analysis Inc., Berlin, Germany) using 150 W Al Kα radiation.

N_2 physisorption at 77 K

The N_2 adsorption–desorption isotherms were obtained at 77 K using an ASAP 2020 automatic apparatus (Micromeritics Instrument Co., Norcross, GA, USA). The samples were degassed for 48 h under vacuum at 523 K prior to the adsorption experiments. Carbon dioxide adsorption was not used to characterize the materials prepared in this study because of the full accessibility of their pores to N_2 at 77 K. Indeed, the porosity was well developed, and no N_2 diffusion limitation was observed. The N_2 adsorption data were obtained and treated as described elsewhere (Luo *et al*. 2017; Zhao *et al*. 2017a,b) to determine the following properties: (i) surface area by the Brunauer-Emmett-Teller (BET) calculation method (S_{BET}); (ii) micropore volume according to the Dubinin-Radushkevich (DR) method ($V_{DR,N2}$); and (iii) total pore volume defined as the volume of liquid nitrogen corresponding to the amount adsorbed at a relative pressure (P/P_0) of 0.99 ($V_{0.99}$). The average micropore diameter (L_0) and pore size distribution (PSD) were also calculated with the density functional theory (DFT).

CO_2 adsorption at 273 K

An ASAP 2020 automatic apparatus (Micromeritics Instrument Co., Norcross, GA, USA) was used for the CO_2 adsorption analysis. The CO_2 adsorption isotherms were determined by dosing CO_2 volumes of 0.2 STP (standard temperature and pressure) cm^3/g up to a $P/\underline{P}_0$ of 10^{-4}, and a P/P_0 table was used to construct the CO_2 adsorption isotherm up to a final P/P_0 of 1. An equilibration time of 50 s was used. The CO_2 data was interpreted based on the DR model with correlation coefficients equal to or higher than 0.999. The micropore volume determined by the CO_2 adsorption data ($V_{DR,CO2}$) provides information about micropores narrower than 0.7 nm. Finally, the PSDs were calculated by applying the DFT model using a Micromeritics ASAP 2020 HD 88 system (Xia *et al*. 2017).

RESULTS AND DISCUSSION

TGA

The carbonization and activation processes of the edamame shell in a N_2 atmosphere were studied by TGA, and the results are given in Fig. 2. The carbonization process curve of the BS had three distinct stages of weight loss. The temperature range of less than 403 K corresponded to the weight loss of physisorbed water. The second stage of remarkable weight loss occurred from 473 K to 673 K and was primarily because of the evaporation of H_2O, and the escape of H and O atoms. Hence, the yield of edamame shell carbonization was 28.5% with an inferred favorable temperature of 723 K, which was similar to that of other biomass charcoals prepared in previous studies (Xu *et al*. 2015; Zhao *et al*. 2017b).

The activation process of the sample with a *W* of 3 (BC13) is shown in Fig. 2, and it had three different stages of mass loss. The first stage of mass loss at less than 393 K correlated to the dehydration of the KOH activation agent. The second stage was nearly a plateau from 393 K to 973 K, which indicated that there may have been no activation reaction. The third stage was observed at high temperatures (973 K to 1193 K) and corresponded to a sharp mass loss that was caused by the reaction of C-KOH. Pores are produced by the removal of C. In general, the chemical reaction between KOH and a carbon material can be written as follows (Rodríguez-Reinoso 2002; Azargohar 2009; Viswanathan *et al*. 2009):

$$4\ KOH + C \rightarrow K_2CO_3 + K_2O + 2\ H_2 \qquad\qquad (1)$$

The activation temperature is an important parameter for preparing ACs. Increasing the activation temperature results in noticeable changes to the porosity of ACs (Yoon *et al.* 2004; Kim *et al.* 2007; Cardoso *et al.* 2008). It was speculated from the TG curve that the appropriate activation temperature could be 1073K, which corresponded to a yield of 64.8%.
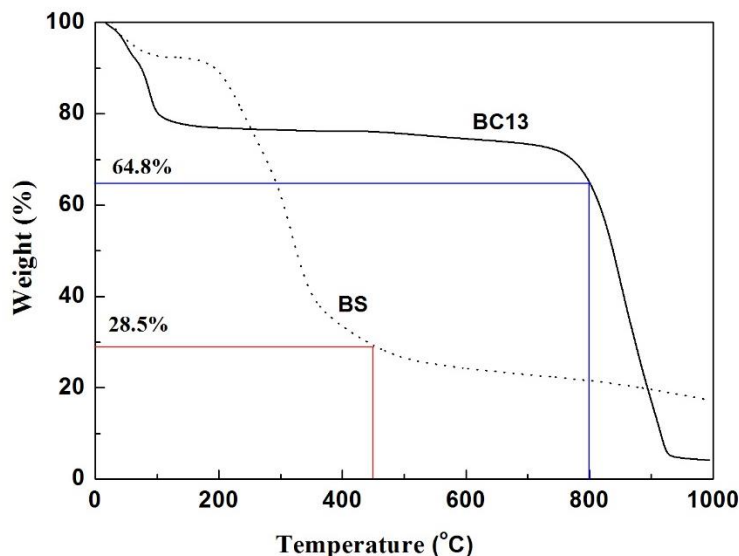

Fig. 2. TG curves of the BS (solid line) and BC13 (dotted line) under a N_2 atmosphere

Elemental Composition of all of the Materials

The elemental analyses of all of the materials prepared at different stages are shown in Table 1. The carbon content of the natural edamame shell used in this work was 42.1%. The carbon content increased remarkably after the carbonization and activation processes, and yielded 62.4% after carbonization and 70.8% to 78.2% after further activation. The N, O, and H contents decreased from 10.0%, 38.4%, and 5.0% to 6.5%, 25.6%, and 4.2% after carbonization, respectively. For the BC samples, the N and O contents were in the range of 1.20 wt% to 1.81 wt% and 5.13 wt% to 9.98 wt%, respectively.

Table 1. Elemental Analysis Results for All of the Samples

Sample	C (wt%)	N (wt%)	O (wt%)	H (wt%)
Edamame shell	42.10	9.99	38.44	5.00
BS	62.44	6.52	25.56	4.25
BC12	70.80	1.81	9.98	2.35
BC13	72.41	1.40	8.30	2.21
BC14	73.56	1.32	8.08	2.02
BC15	75.82	1.31	7.58	1.56
BC16	78.21	1.20	5.13	1.30

As was expected, pyrolysis caused a major decrease in the N, O, and H contents, but the N and O atoms were successfully incorporated into the C framework. The challenge for synthesizing N/O-doped carbon materials was to prepare materials that had both a high porosity and high N content because N is a volatile element that changes more easily with an increase in the heat-treatment temperature and/or the porosity of the material in which it is contained (Boudou 2003; Hulicova-Jurcakova *et al.* 2009; Xia *et al*. 2011; Zhao *et al.* 2013; Luo *et al.* 2017).

XPS Analysis

The XPS analysis was intensively utilized to investigate the elemental composition and chemical states. Figure 3A shows that the full survey spectra of the BS and BC13 all included obvious peaks ascribed to the C 1s (284.56 eV), N 1s (400.15 eV), and O 1s (532.23 eV) orbitals, and no other impurity peaks were observed, which validated the compositional analysis of the C, O, and N elements. The C, N, and O contents of the edamame shell were 62.2%, 10.4%, and 27.3%, respectively. The C content increased obviously up to 80.4%, while N and O contents decreased to 7.2% and 12.4% after carbonization. At the end, after activation, the C, N, and O contents for BC13 were 95.0%, 3.7%, and 1.3%, respectively. During carbonization, the C content increased considerably, and the O and N contents decreased due to the evaporation of H, N, and O in the gas phase (Braghiroli *et al.* 2012). Then, during thermal activation at high temperatures, the KOH activation involved the reaction of C and KOH *via* Eq. 1. Additionally, the abundant O functional groups in the biochar can react with the KOH during heating to generate H_2O, CO_2, and NOx gases because of dehydration, denitrogenation, and decarboxylation (Rodríguez-Reinoso 2002). This demonstrated that the carbonization and activation processes caused more obvious denitrogenation and deoxygenation of BC13 accompanied by the pore creation effect. The XPS results confirmed that the N and O atoms were successfully incorporated into the C framework, which was also in agreement with the elemental analysis results.

The results of the C, O, and N analysis were studied by peak-differentiating and imitating to determine the detailed bonding configurations. According to previous literature (Boudou 2003; Hulicova-Jurcakova *et al.* 2009; Xia *et al*. 2011; Zhao *et al.* 2013; Gao *et al*. 2015; Xu *et al*. 2015; Zhai *et al.* 2016; Luo *et al.* 2017), the regions corresponding to N 1s binding energies in carbon materials are 398.5 eV ± 0.4 eV for pyridinic-N (N-6), 400.5 eV ± 0.3 eV for pyrrolic-N (N-5), 400.5 eV for pyridinic-N (N-6(O)), 399.6 eV ± 0.2 eV for pyrrolidinic-N (N-5(O)), 401.1 eV ± 0.3 eV for quaternary-N (N-Q), and 402.5 eV to 403.7 eV for pyridinic-N-oxide (N-X). Figures 3F and 3G show the N 1s peak of BC13 that can be divided into three components, which corresponded to pyridinic-N (N-6, approximately 398.3 eV), pyrrolic-N (N-5, approximately 399.8 eV), and quaternary-N (N-Q, approximately 401.5 eV). The C 1s spectrum displayed an asymmetric shape in Figs. 3B and 3C, with the four components of the C species corresponding to C-C/C=C at 284.6 eV, C-OH/C-O-C at 285.3 eV, C=O/C-N at 286.2 eV, and C(O)OH/C(O)-O-C at 288.5 eV in the BS and BC13. Among them, three of the C peak areas (C-N/C-O, C=N/C=O, and –O-C=O) decreased and the C=C peak area increased during KOH activation, which agreed with the conclusion that the N and O contents were reduced during activation. Figures 3D and 3E show the O 1s spectrum with three O components, which were C=O at 531.7 eV, C-OH at 532.8 eV, and –COOH at 533.4 eV. It was obvious that for the O 1s spectrum, the C=O and C-OH peak intensities increased and decreased after activation, respectively.
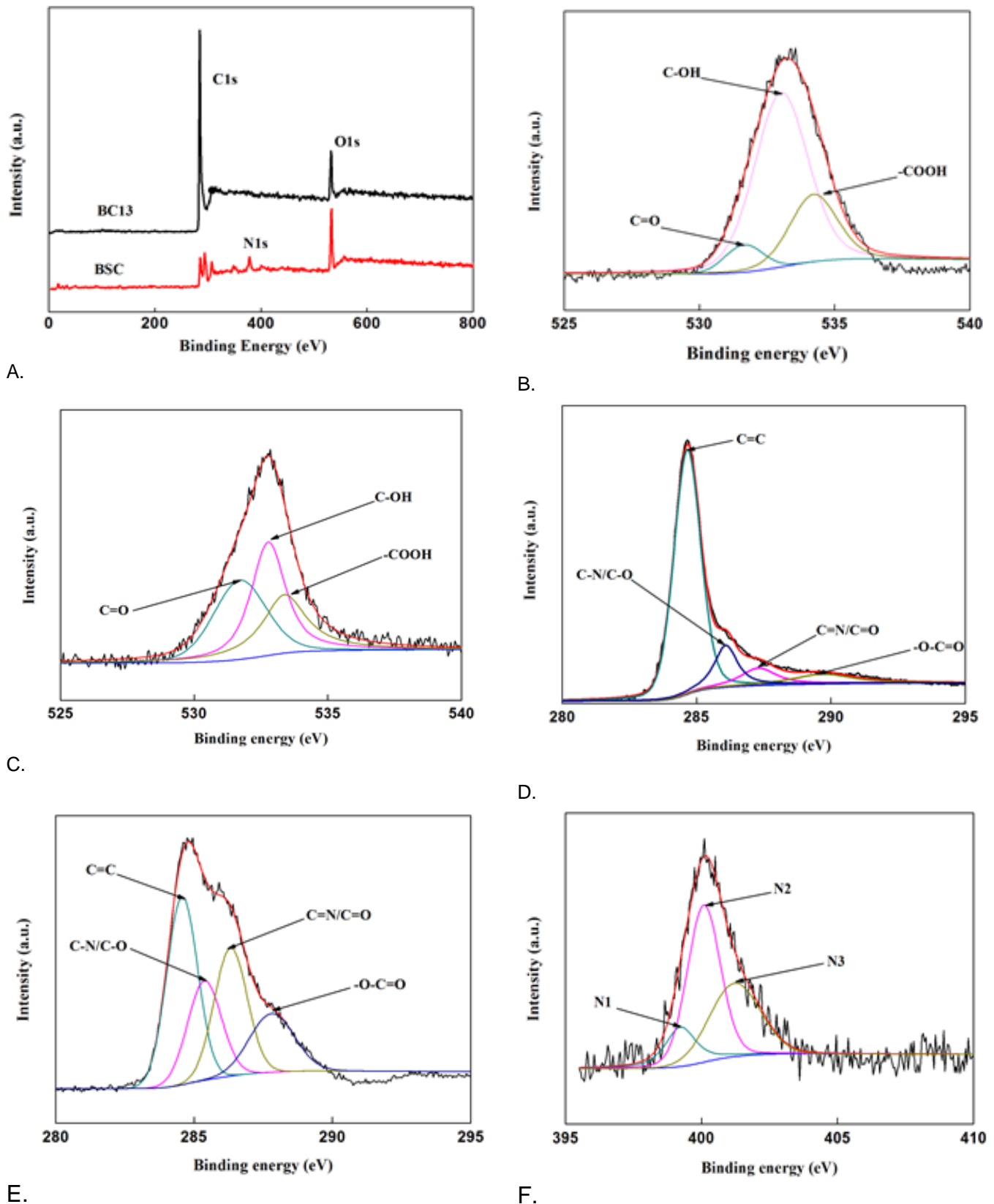
***bioresources*.com**

Fig. 3A-F. XPS survey of the BS and BC13 (A); C 1s (B), O 1s (D), and N 1s (F) core-level spectra of the BS; and C 1s (C), O 1s (E), and N 1s (G) core-level spectra of BC13

Fig. 3G. XPS survey of the BS and BC13 (A); C 1s (B), O 1s (D), and N 1s (F) core-level spectra of the BS; and C 1s (C), O 1s (E), and N 1s (G) core-level spectra of BC13
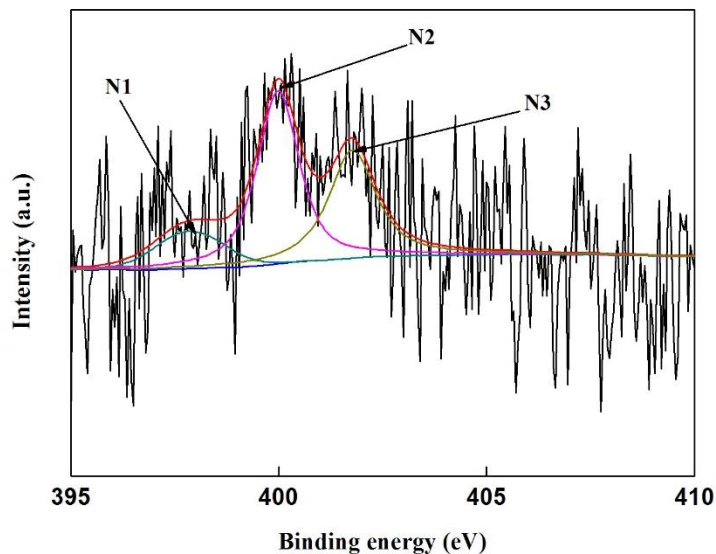
Morphology Analysis

Figure 4 shows the material morphology of the edamame shell, BS, and BC13 determined by SEM. The representative SEM image in Fig. 4a shows that the surface of the edamame shell exhibited a plant fiber structure that was rough and heterogeneous with a rugged morphology. The morphology of the BS in Fig. 4b was entirely different from the edamame shell; it contained many cavities with a heterogeneous porous structure, which was attributed to the evaporation during the carbonization process. Figures 4c through 4e show SEM images of the resultant BC13 at different magnifications. Serious structural changes were induced, which indicated that the prepared porous carbon sample possessed a continuous branched porous framework that consisted of C nanosheets and fully interconnected pores that ranged from several nanometers to hundreds of nanometers in size. The porous sheet-like structure was further studied by HRTEM (Fig. 4f), which illustrated and proved the amorphous and microporous structures of the AC sample. These results were in good agreement with the results from the N_2 adsorption/desorption analysis that showed that the S_{BET} obviously increased after carbonization and activation.

Porous Texture

Figure 5a shows the N_2 adsorption–desorption isotherms of the ACs from various W values. All the N_2 isotherms were type I according to the International Union of Pure and Applied Chemistry (IUPAC) classification system (Rodríguez-Reinoso 2002). The type I isotherm is common to microporous materials with a narrow range of pore distributions. The key features of type I isotherms for these microporous materials are a sharp increase in the N_2 adsorption capacity at a very low P/P_0 (lower than 0.05), almost a plateau at a higher P/P₀, and no adsorption–desorption hysteresis cycle. As the W increased from 2 to 6, the knee of the isotherm widened, which indicated a broadening of the micropore width. The CO_2 adsorption isotherms of all ACs are shown in Fig. 5b. It was obvious that the total adsorbed CO_2 volume first increased and then decreased, which indicated a decrease in the number of the narrowest micropores with a higher W.
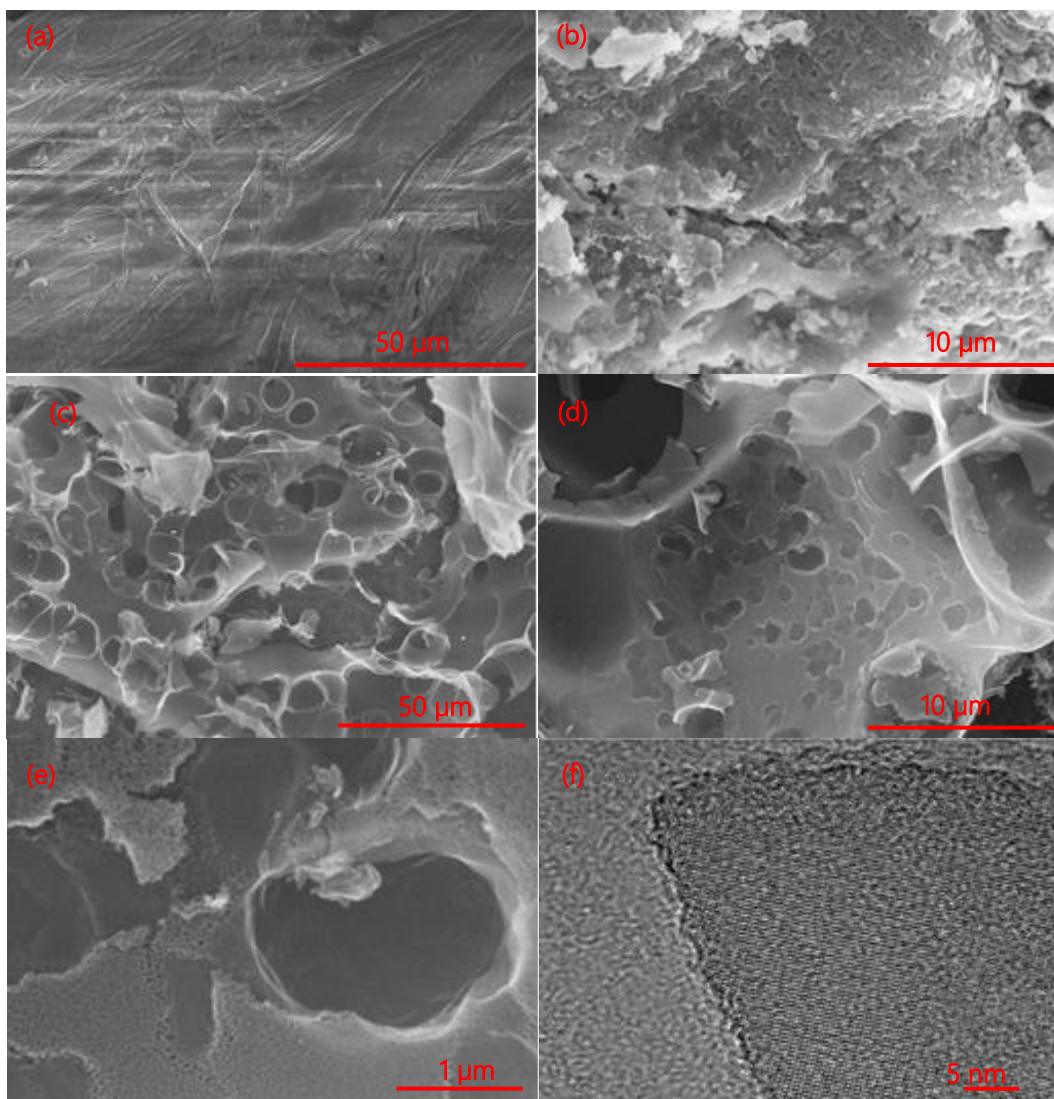
Fig. 4. SEM images of the edamame shell (a), BS (b), and BC13 (c, d, and e); and TEM image of BC13 (f)

Table 2 contains the mathematical treatment results of the N_2 adsorption data for the S_{BET}, $V_{0.99}$, $V_{DR,N2}$, L_0, and mesopore volume (V_{meso}). Furthermore, the micropore structure was investigated with CO_2 adsorption–desorption at 273 K because of cardinal importance, and the results of that micropore volume ($V_{DR,CO2}$) are also shown in Table 2. It was found that during the activation process, the redox reactions between the K compounds and C resulted in a major increase in the S_{BET}, which ranged from 1135 m^2/g to 1835 m^2/g. The $V_{DR,N2}$ increased with the S_{BET}, and ranged from 0.46 cm^3/g to 0.70 cm^3/g. The W was determined as the most important parameter in the KOH chemical activation process. Increasingly high values of W led to increased S_{BET} values and pore volumes until a maximum was reached, and then the pore texture parameters started to decrease (Rodríguez-Reinoso 2002). These results are in good agreement with prior studies that showed that the S_{BET} and $V_{DR,N2}$ increased until a certain W, and then decreased with higher W values. An S_{BET} of 1835 m^2/g was obtained when the W was 3. The destruction of the pore structure caused by excessive KOH treatment (higher W values). The prepared BCs

had a $V_{0.99}$ that ranged from 0.53 cm^3/g to 0.93 cm^3/g. The average L_0 varied from 1.16 nm to 1.33 nm. All of the ACs were mainly microporous because the $V_{DR,N2}/V_{0.99}$ ranged from 0.72 to 0.87, which confirmed the results of the N$_2$ isotherms and PSD. The range of $V_{DR,CO2}$ values (0.13 cm^3/g to 0.18 cm^3/g) were much lower than the range of $V_{DR,N2}$ values, and no correlation was found between the $V_{DR,CO2}$ and S_{BET}.
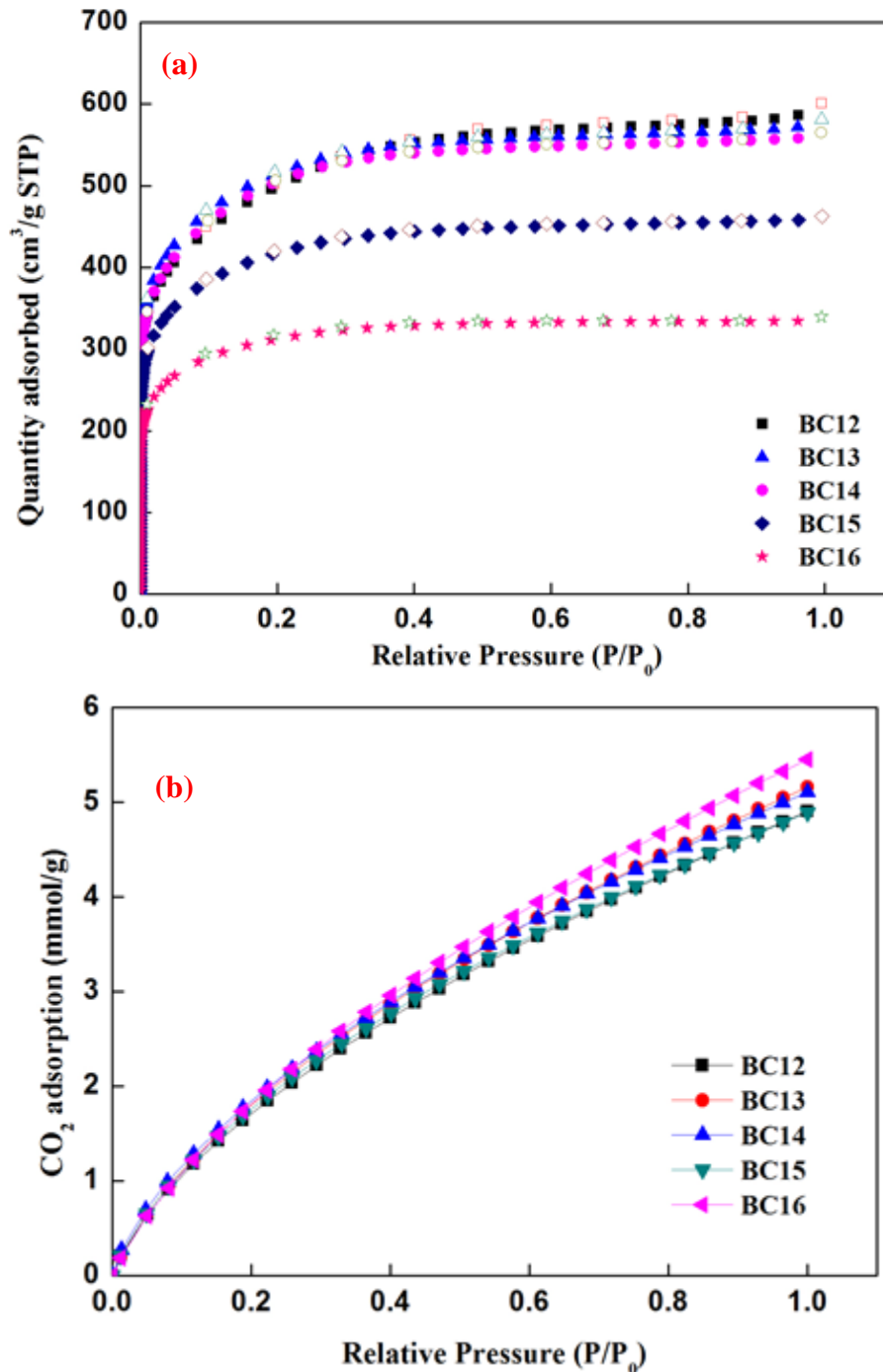

Fig. 5. Adsorption (full symbols)-desorption (open symbols) isotherms of the five investigated BCs as a function of the P/P$_0$: (a) N$_2$ isotherms at 77 K and (b) CO$_2$ isotherms at 273 K

Table 2. Pore Texture Parameters of the BCs Derived from the N_2 and CO_2 Adsorption Data

Sample	W	S_{BET} (m²/g)	$V_{0.99}$ (cm³/g)	V_{DR} (cm³/g)		L_0 (nm)	$V_{DR,N2}/V_{0.99}$	V_{meso} (cm³/g)
				CO_2	N_2			
BC12	2	1786	0.93	0.13	0.67	1.31	0.72	0.26
BC13	3	1835	0.82	0.18	0.70	1.26	0.85	0.12
BC14	4	1809	0.87	0.18	0.67	1.33	0.77	0.20
BC15	5	1522	0.72	0.17	0.59	1.21	0.82	0.13
BC16	6	1135	0.53	0.15	0.46	1.16	0.87	0.07
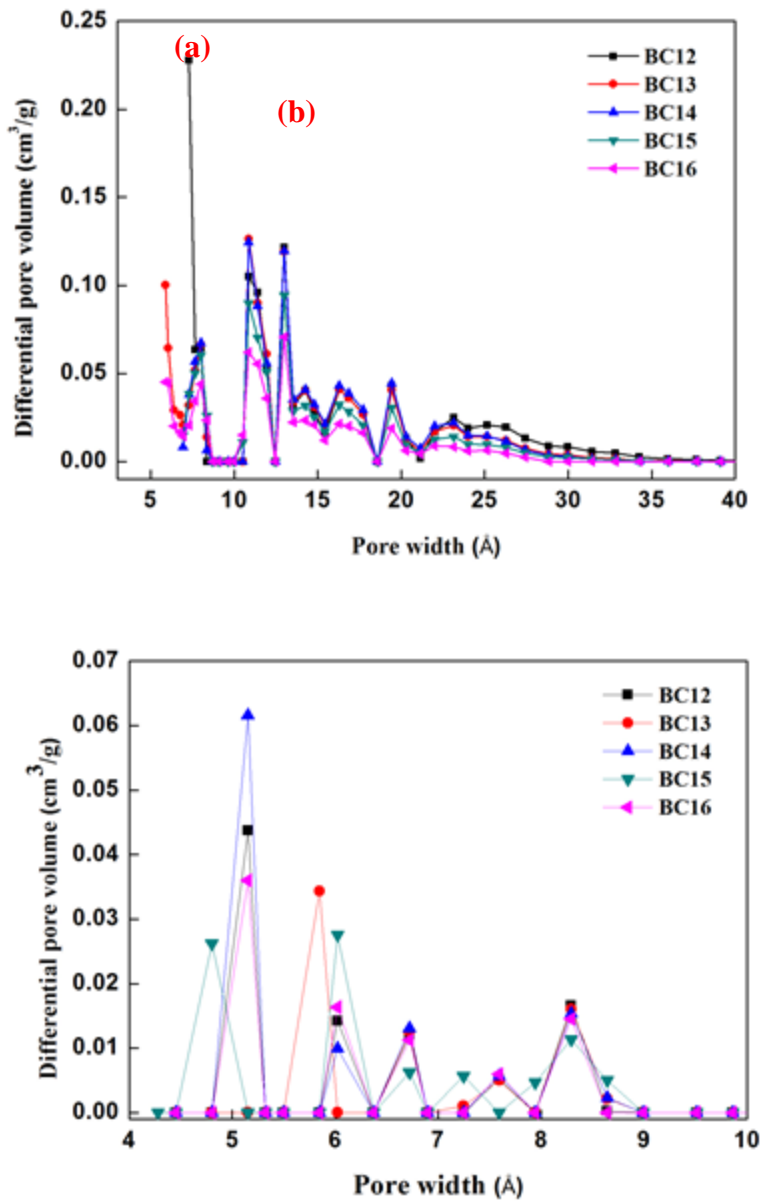
Fig. 6. PSDs calculated from the (a) N_2 adsorption isotherms at 77 K and (b) CO_2 adsorption isotherms at 273 K

bioresources.com

Table 3. Comparison of ACs Doped with Nitrogen

Feedstock	Doping Treatment	S_{BET} (cm²/g)	$V_{0.99}$ (cm³/g)	V_{DR} (cm³/g)	N Content (wt%)	Reference
Shell (a)	Without	1835	0.82	0.70	1.4	This work
Board bean (a)	Without	655	0.38	-	2.0	Xu *et al.* (2015)
Sweet potato vine (a)	Without	885	0.52	0.40	1.2	Gao *et al.* (2015)
Resin containing N (b)	Without	1674	-	0.86	1.50	Zhao *et al.* (2017a)
Aminophenol/formaldehyde resin (b)	Without	226	0.18	0.08	4.06	Li *et al.* (2015)
Polyaniline (b)	Without	1805	0.64	-	3.2	Silvestre-Albero *et al.* (2015)
Polyphosphazene (b)	Without	1341	0.69	-	5.4	Zhou *et al.* (2015)
Sodium alginate/ polyaniline (b)	Without	-	-	-	3.48	Ye *et al.* (2017)
Polypyrrole (b)	Without	398	0.16	-	3.29	Meng *et al.* (2014)
Particleboard containing urea resin (c)	Urea	1433	0.82	0.65	1.83	Shang *et al.* (2015)
Particleboard containing urea resin (c)	Urea	1360	0.78	0.61	1.81	Shang *et al.* (2015)
Particleboard containing urea resin (c)	Urea	1344	0.77	0.60	1.77	Shang *et al.* (2015)
Luffa sponge fibers treated with NH$_3$ (c)	NH$_3$	1694	0.76	0.51	0.55	Li *et al.* (2014)
Melamine-modified PF resins (c)	Melamine	1439	0.75	0.6	1.00	Tseng *et al.* (2015)
AC from coconut shell (d)	Urea	808 (898*)	-	0.406	2.9	Hulicova-Jurcakova *et al.* (2009)
AC from coconut shell (d)	Melamine	732 (898*)	-	0.372	4.0	Hulicova-Jurcakova *et al.* (2009)
AC from anthracite (d)	Urea	2082 (2527*)	0.89	0.72	7.8	Zhao *et al.* (2013)
AC from wood (d)	Melamine	874 (1549*)	0.83	0.32	-	Travlou *et al.* (2016)
AC from resin (d)	NH$_3$ gas	1736 (2054*)	0.72	0.27	4.99	Chen *et al.* (2014)
AC from resin (d)	NH$_3$ gas	2039 (2054*)	0.88	0.28	7.17	Chen *et al.* (2014)
AC from resin (d)	NH$_3$ gas	1332 (2054*)	0.63	0.19	3.98	Chen *et al.* (2014)
ACs from RF gels (d)	NaNH$_2$/NH$_4$Cl	1938 (2186*)	1.52	-	1.60	Hasegawa *et al.* (2015)

* Value in parentheses is the surface area of the AC after N-doping

Figures 6a and 6b show the PSDs derived from the N_2 and CO_2 adsorption experiments, respectively. The results corroborated the aforementioned conclusion that N- and O-doped ACs are mainly microporous materials and higher *W* values causes the pore structure destruction.

Comparison with the Literature

As previously mentioned, the methods for heteroatom doping are usually very similar. Table 3 summarizes typical N-doped ACs prepared for comparison. Four approaches to fabricate N-doped ACs have been developed: (a) the use of biomass materials that contain N; (b) synthesis of polymers from N-containing raw materials, followed by carbonization and activation processes; (c) pre-treatment of the precursors with reactive heteroatom sources, followed by a carbonization/activation process; and (d) post-treatment of ACs with reactive heteroatom sources. First, it has been demonstrated that methods (b) and (d) can obtain ACs with higher N contents than the other methods. However, the use of toxic reactive gases (*e.g.*, NH_3 or HCN for N-doping) causes hesitation among researchers. The other methods use a solid reactant as a source of N, such as urea and melamine, but it does not apply to monolithic carbons. Meanwhile, for method (b), the process of developing a polymer is very complicated, which increases the cost of the final product. Furthermore, the post-treatment method (d) not only modifies the surface chemistry of the ACs, but also their porous texture. Pores that are produced by activation may be blocked by the heteroatom sources. There was a distinct decrease in the specific surface area after post-treatment with reactive heteroatom sources, although the N content was higher than for the other methods. In contrast, method (a) presented a lower N content than method (c) because denitrogenation takes place during the carbonization and activation processes, but it eliminates the need for pre-treatment to achieve N-doping. As a result, it is essential and important that a new resource be found, especially a biomass material containing a high N content. The advantage of using edamame shell as a precursor for producing ACs because of the low cost and relative high N content. The ACs prepared from edamame shell show comparable surface areas and relatively lower N contents with the results from open literatures, no matter the preparation methods.

CONCLUSIONS

1. Edamame shell contains an abundance of N (9.99 wt. %) that results from the nitrogen fixation property of legumes, as well as O (38.4 wt. %), which is an ideal precursor for preparing N and O self-doped porous carbons.

2. The N and O contents of the prepared ACs were in the range of 1.20 wt.% to 1.81. wt.% and 5.13 wt.% to 9.98 wt.%, respectively.

3. An S_{BET} of 1835 m^2/g, high N and O contents of approximately 1.4 wt% and 8.3 wt%, respectively, and mainly microporosity were achieved when the W was 3.

4. The N/O codoped microporous ACs produced by KOH activation were obtained from edamame shell without any dopant reagent, which is a facile and cost-effective method to successfully obtain heteroatom doped ACs with high surface areas.

ACKNOWLEDGMENTS

REFERENCES CITED

Ahmad, M. A., Puad, N. A. A., and Bello, O. S. (2014). "Kinetic equilibrium and thermodynamic studies of synthetic dye removal using pomegranate peel activated carbon prepared by microwave-induced KOH activation," *Water Resources and Industry* 6, 18-35. DOI: 10.1016/j.wri.2014.06.002

Alabadi, A., Abbood, H. A., Li, Q., Jing, N., and Tan, B. (2016). "Imine-linked polymer based nitrogen-doped porous activated carbon for efficient and selective CO_2 capture," *Sci. Rep.-UK* 6, Article ID 38614. DOI: 10.1038/srep38614

Azargohar, R. (2009). *Production of Activated Carbon and its Catalytic Application for Oxidation of Hydrogen Sulphide*, Ph.D. Thesis, University of Saskatchewan, Saskatoon, Canada.

Braghiroli, F. L., Fierro, V., Izquierdo, M. T., Parmentier, J., Pizzi, A., and Celzard, A. (2012). "Nitrogen-doped carbon materials produced from hydrothermally treated tannin," *Carbon* 50(15), 5411-5420. DOI: 10.1016/j.carbon.2012.07.027

Boudou, J. P. (2003). "Surface chemistry of a viscose-based activated carbon cloth modified by treatment with ammonia and steam," *Carbon* 41(10), 1955-1963. DOI: 10.1016/S0008-6223(03)00182-9

Cardoso, B., Mestre, A. S., Carvalho, A. P., and Pires, J. (2008). "Activated carbon derived from cork powder waste by KOH activation: Preparation, characterization, and VOCs adsorption," *Ind. Eng. Chem. Res.* 47(16), 5841–5846. DOI: 10.1021/ie800338s

Chen, L.-C., Peng, O.-Y., Lin, L.-F., Yang, T. C. K., and Huang, C.-M. (2014). "Facile preparation of nitrogen-doped activated carbon for carbon dioxide adsorption," *Aerosol Air Qual. Res.* 14(3), 916-927. DOI: 10.4209/aaqr.2013.03.0089

Ci, E., and Gao, M. (2005). "Research advances in the effects of environmental factors on the symbiotic nitrogen fixation of legumes," *Acta Botanica Boreali-Occidentalia Sinica* 25(6), 1269-1274.

Dang, Y., Guo, W., Zhao, L., and Zhu, H. (2017). "Porous carbon materials based on graphdiyne basis units by the incorporation of the functional groups and Li atoms for superior CO_2 capture and sequestration," *ACS Appl. Mater. Inter.* 9(35), 30002-30013. DOI: 10.1021/acsami.7b10836

Gao, F., Qu, J., Zhao, Z., Wang, Z., and Qiu, J. (2016). "Nitrogen-doped activated carbon derived from prawn shells for high-performance supercapacitors," *Electrochim. Acta* 190, 1134-1141. DOI: 10.1016/j.electacta.2016.01.005

Gao, S., Li, L., Geng, K., Wei, X., and Zhang, S. (2015). "Recycling the biowaste to produce nitrogen and sulfur self-doped porous carbon as an efficient catalyst for oxygen reduction reaction," *Nano Energy* 16, 408-418. DOI: 10.1016/j.nanoen.2015.07.009

Hasegawa, G., Deguchi, T., Kanamori, K., Kobayashi, Y., Kageyama, H., Abe, T., and Nakanishi, K. (2015). "ChemInform abstract: High-level doping of nitrogen,

phosphorus, and sulfur into activated carbon monoliths and their electrochemical capacitances," *ChemInform* 46(38). DOI: 10.1002/chin.201538008

Hulicova-Jurcakova, D., Seredych, M., Lu, G. Q., and Bandosz, T. J. (2009). "Combined effect of nitrogen- and oxygen- containing functional groups of microporous activated carbon on its electrochemical performance in supercapacitors," *Adv. Funct. Mater.* 19(3), 438-447. DOI: 10.1002/adfm.200801236

Hwang, J. Y., Li, M., El-Kady, M. F., and Kaner, R. B. (2017). "Next-generation activated carbon supercapacitors: A simple step in electrode processing leads to remarkable gains in energy density," *Adv. Funct. Mater.* 27(15). DOI: 10.1002/adfm.201605745

Jiang, L., Wang, J., Mao, X., Xu, X., Zhang, B., Yang, J., Wang, Y., Zhu, J., and Hou, S. (2017). "High rate performance carbon nano-cages with oxygen-containing functional groups as supercapacitor electrode materials," *Carbon* 111, 207-214. DOI: 10.1016/j.carbon.2016.09.081

Karnan, M., Subramani, K., Sudhan, N., Ilayaraja, S., and Sathish, M. (2016). "*Aloe vera* derived activated high-surface-area carbon for flexible and high-energy supercapacitors," *ACS Appl. Mater. Inter.* 8(51), 35191-35202. DOI: 10.1021/acsami.6b10704

Li, J., Wang, S., Ren, Y., Ren, Z., Qiu, Y., and Yu, J. (2014). "Nitrogen-doped activated carbon with micrometer-scale channels derived from luffa sponge fibers as electrocatalysts for oxygen reduction reaction with high stability in acidic media," *Electrochim. Acta* 149, 56-64. DOI: 10.1016/j.electacta.2014.10.089

Li, Y.-F., Liu, Y.-Z., Liang, Y., Guo, X.-H., and Chen, C.-M. (2017). "Preparation of nitrogen-doped graphene/activated carbon composite papers to enhance energy storage in supercapacitors," *Appl. Phys. A-Mater.* 123(9), 566. DOI: 10.1007/s00339-017-1178-9

Li, Y., Zhang, S., Song, H., Chen, X., Zhou, J., and Hong, S. (2015). "New insight into the heteroatom-doped carbon as the electrode material for supercapacitors," *Electrochim. Acta* 180, 879-886. DOI: 10.1016/j.electacta.2015.09.039

Liu, L., Zhang, L. G., and Hu, Z. (2014). "Emergency response technology using powdered activated carbon for sudden water pollution accidents with petroleum pollutants," *Adv. Mater. Res.* 955-959, 2517-2520. DOI: 10.4028/www.scientific.net/AMR.955-959.2517

Luo, L., Chen, T., Zhao, W., and Fan, M. (2017). "Hydrothermal doping of nitrogen in bamboo-based super activated carbon for hydrogen storage," *BioResources* 12(3), 6237-6250. DOI: 10.15376/biores.12.3.6237-6250

Kim, B.-J., Lee, Y.-S., and Park, S.-J. (2007). "A study on pore-opening behaviors of graphite nanofibers by a chemical activation process," *J. Colloid. Interf. Sci.* 306(2), 454-458. DOI: 10.1016/j.jcis.2006.10.038

Ma, C., Chen, X., Long, D., Wang, J., Qiao, W., and Ling, L. (2017). "High-surface-area and high-nitrogen-content carbon microspheres prepared by a pre-oxidation and mild KOH activation for superior supercapacitor," *Carbon* 118, 699-708. DOI: 10.1016/j.carbon.2017.03.075

Meng, Y., Zou, X., Huang, X., Goswami, A., Liu, Z., and Asefa, T. (2014). "Polypyrrole-derived nitrogen and oxygen co-doped mesoporous carbons as efficient metal-free electrocatalyst for hydrazine oxidation," *Adv. Mater.* 26(37), 6510-6516. DOI: 10.1002/adma.201401969

Ren, D. W., Wang, E. T., Chen, W. F., Sui, X. H., Zhang, X. X., Liu, H. C., and Chen,

W. X. (2011). "*Rhizobium herbae* sp. nov. and *Rhizobium giardinii*-related bacteria, minor microsymbionts of various wild legumes in China," *Int. J. Syst. Evol. Micr.* 61, 1912-1920. DOI: 10.1099/ijs.0.024943-0

Rodríguez-Reinoso, F. (2002). "Production and applications of activated carbons," in: *Handbook of Porous Solids*, F. Schüth, K. S. W. Sing, and J. W. (eds.), Wiley-VCH Verlag GmbH, Weinheim, Germany, pp. 1766-1827. DOI: 10.1002/9783527618286.ch24a

Şahin, Ö., and Saka, C. (2013). "Preparation and characterization of activated carbon from acorn shell by physical activation with H_2O-CO_2 in two-step pretreatment," *Bioresource Technol.* 136, 163-168. DOI: 10.1016/j.biortech.2013.02.074

Shang, T. X., Cai, X. X., and Jin, X. J. (2015). "Phosphorus- and nitrogen-co-doped particleboard based activated carbon in supercapacitor application," *RSC Adv.* 5(21), 16433-16438. DOI: 10.1039/C5RA00142K

Silvestre-Albero, A., Silvestre-Albero, J., Martinez-Escandell, M., Molina-Sabio, M., Kovacs, A., and Rodriguez-Reinoso, F. (2015). "Novel synthesis of a micro-mesoporous nitrogen-doped nanostructured carbon from polyaniline," *Micropor. Mesopor. Mat.* 218, 199-205. DOI: 10.1016/j.micromeso.2015.07.023

Tai, Z., Zhang, Q., Liu, Y., Liu, H., and Dou, S. (2017). "Activated carbon from the graphite with increased rate capability for the potassium ion battery," *Carbon* 123, 54-61. DOI: 10.1016/j.carbon.2017.07.041

Travlou, N. A., Ushay, C., Seredych, M., Rodríguez-Castellón, E., and Bandosz, T. J. (2016). "Nitrogen-doped activated carbon-based ammonia sensors: Effect of specific surface functional groups on carbon electronic properties," *ACS Sensors* 1(5), 591-599. DOI: 10.1021/acssensors.6b00093

Tseng, R.-L., Wu, F.-C., and Juang, R.-S. (2015). "Adsorption of CO_2 at atmospheric pressure on activated carbons prepared from melamine-modified phenol–formaldehyde resins," *Sep. Purif. Technol.* 140, 53-60. DOI: 10.1016/j.seppur.2014.11.018

Viswanathan, B., Neel, P. I., and Varadarajan, T. K. (2009). *Methods of Activation and Specific Applications of Carbon Materials*, National Center for Catalysis Research, Indian Institute of Technology Madras, Chennai, India.

Wani, S. P., Rupela, O. P., and Lee, K. K. (1995). "Sustainable agriculture in the semi-arid tropics through biological nitrogen fixation in grain legumes," *Plant Soil* 174(1-2), 29-49. DOI: 10.1007/BF00032240

Xia, Y., Mokaya, R., Grant, D. M., and Walker, G. S. (2011). "A simplified synthesis of N-doped zeolite-templated carbons, the control of the level of zeolite-like ordering and its effect on hydrogen storage properties," *Carbon* 49(3), 844-853. DOI: 10.1016/j.carbon.2010.10.028

Xia, K., Li, Q., Zheng, L., You, K., Tian, X., Han, B., Gao, Q., Huang, Z., Chen, G., and Zhou, C. (2017). "Controllable fabrication of 2D and 3D porous graphene architectures using identical thermally exfoliated graphene oxides as precursors and their application as supercapacitor electrodes," *Micropo. Mesopo. Mat.* 237, 228-236. DOI: 10.1016/j.micromeso.2016.09.015

Xu, G., Han, J., Ding, B., Nie, P., Pan, J., Dou, H., Li, H., and Zhang, X. (2015). "Biomass-derived porous carbon materials with sulfur and nitrogen dual-doping for energy storage," *Green Chem.* 17(3), 1668-1674. DOI: 10.1039/C4GC02185A

Yamashita, A., Okamoto, M., Ishikawa, M., and Oda, H. (2006). "Modification of functional group on porous carbon materials and its characteristics: Effect on

bioresources.com

capacitance," *Hyomen Kagaku* 27(8), 461-468. DOI: 10.1380/jsssj.27.461

Ye, Z., Wang, F., Jia, C., Mu, K., Yu, M., Lv, Y., and Shao, Z. (2017). "Nitrogen and oxygen-codoped carbon nanospheres for excellent specific capacitance and cyclic stability supercapacitor electrodes," *Chem. Eng. J.* 330, 1166-1173. DOI: 10.1016/j.cej.2017.08.070

Yoon, S.-H., Lim, S., Song, Y., Ota, Y., Qiao, W., Tanaka, A., and Mochida, I. (2004). "KOH activation of carbon nanofibers," *Carbon* 42(8-9), 1723-1729. DOI: 10.1016/j.carbon.2004.03.006

Zhai, Y., Xu, B., Zhu, Y., Qing, R., Peng, C., Wang, T., Li, C., and Zeng, G. (2016). "Nitrogen-doped porous carbon from *Camellia oleifera* shells with enhanced electrochemical performance," *Mat. Sci. Eng. C-Mater.* 61, 449-456. DOI: 10.1016/j.msec.2015.12.079

Zhang, J., Zhong, Z., Shen, D., Zhao, J., Zhang, H., Yang, M., and Li, W. (2011). "Preparation of bamboo-based activated carbon and its application in direct carbon fuel cells," *Energ. Fuel.* 25(5), 2187-2193. DOI: 10.1021/ef200161c

Zhao, W., Fierro, V., Fernández-Huerta, N., Izquierdo, M. T., and Celzard, A. (2013). "Hydrogen uptake of high surface area-activated carbons doped with nitrogen," *Int. J. Hydrogen Energ.* 38(25), 10453-10460. DOI: 10.1016/j.ijhydene.2013.06.048

Zhao, W., Luo, L., and Fan, M. (2017a). "Preparation and characterization of nitrogen-containing cellular activated carbon for CO_2 and H_2 adsorption," *Nano* 12(1), 5778-5787. DOI: 10.1142/S1793292017500072

Zhao, W., Luo, L., Wang, H., and Fan, M. (2017b). "Synthesis of bamboo-based activated carbons with super-high specific surface area for hydrogen storage," *BioResources* 12(1), 1246-1262. DOI: 10.15376/biores.12.1.1246-1262

Zhou, J., Zhang, Z., Xing, W., Yu, J., Han, G., Si, W., and Zhuo, S. (2015). "Nitrogen-doped hierarchical porous carbon materials prepared from meta-aminophenol formaldehyde resin for supercapacitor with high rate performance," *Electrochim. Acta* 153, 68-75. DOI: 10.1016/j.electacta.2014.11.075